Time-Domain Analysis of the TALOS Wave Energy Converter using different Computational Tools

Constantine Michailides[1], Eva Loukogeorgaki[2], Wanan Sheng[3] and George Aggidis[3]
[1]Department of Civil Engineering, International Hellenic University
Serres University Campus, Greece
[2]Department of Civil Engineering, Aristotle University of Thessaloniki
Thessaloniki, Greece
[3]Renewable Energy Group and Fluid Machinery Group, Engineering Department, Lancaster University
Lancaster, UK

ABSTRACT

This paper focuses on the preliminary time-domain analysis of a multi-mode Wave Energy Converter (WEC), the so-called TALOS WEC, by deploying two different computational tools. The device consists of an internal sphere attached to its floater with springs and dampers, and power is captured through the sphere's motions relatively to the floater. The equation of motion is formed based on the Cummins formulation using different calculation approaches for the convolution terms in the two tools. A comparative study, initially, is conducted assuming rigid connection of the sphere with the floater. Next, by enabling the sphere to oscillate in heave, as well as in both heave and surge, the device's performance for one and two operational modes is assessed.

KEY WORDS: Wave energy; multi-mode WEC; TALOS, time-domain, responses, power.

INTRODUCTION

Wave energy corresponds to a vast, clean source of ocean renewable energy. Its strategic-driven exploitation, as reflected in the EU's Offshore Energy Strategy with the 2030 deployment target of 1 GW for both wave and tidal energy (European Commission, 2020), can accelerate the decarbonization of Europe's power supply, advance the realization of a diverse energy supply and complement existing variable generation to balance grids (Collombet and Cagney, 2022). Accordingly, the wave energy sector during the last decades is rapidly growing and a variety of Wave Energy Converters (WECs) with different working principles have been investigated, developed and tested (Rusu and Onea, 2018; Guo and Ringwood, 2021). Among the existing WECs types, Point Absorbers (PAs) correspond nowadays to the most advanced and research-focused wave energy technology that usually harness wave power only through the heave or pitch oscillations of their floater (Guo et al., 2022). These WECs are characterized by design, manufacturing, deployment and operation simplicity; however, their single-mode operational feature leads to reduced energy extraction ability under off-resonance conditions and narrow power capture bandwidth (Huang et al., 2019).

In order to tackle the latter drawbacks, multi-mode PAs, offering the advantage of energy extraction from more than one oscillation modes, could be developed and deployed. However, up to now, there exist quite limited studies dealing with those devices and demonstrating their increased power absorption ability compared to single-mode PAs. Specifically, Zhang et al. (2013), Zhang et al. (2015), and Tan et al. (2021) investigated numerically and/or experimentally 3-mode PAs, oscillating and operating in heave, surge and pitch, with a Power-Take Off (PTO) mechanism modeled as a linear damping system of 3 Degrees of Freedom (DoFs). A 3-mode PA has been also examined numerically by Huang et al. (2019), with emphasis on the effect of different, non-linear and linear, 3-DoFs PTO mechanisms on the performance of the device. Ye and Chen (2017) proposed a 6-DoFs PA with a 6-PSS (Prismatic pair-Spherical pair–Spherical pair) PTO mechanism and assessed numerically the performance of a simplified 3-mode PA that oscillates in heave, surge and pitch and has an idealized 3-DoFs linear damping system for the PTO mechanism.

A novel multi-mode PA, the so-called TALOS WEC (Fig. 1), which is the focus of the present paper, corresponds to part of ongoing research and development activities on wave energy conversion at Lancaster University (Aggidis and Taylor, 2017). The device has a 6-DoFs rigid floater and a PTO mechanism enclosed inside the hull; hence, all mechanical components are not exposed to the harsh marine environment. Unlike the traditional PTO mechanisms, the TALOS internal PTO system consists of an inertial mass (sphere) attached to the floater with springs and dampers (e.g., hydraulic cylinders), while power is absorbed through the relative motions between the sphere and the floater. So, depending upon the arrangement of the multiple spring-

damper system's components, the TALOS device can extract power by exploiting the relative sphere-floater motions ideally in all six DoFs.
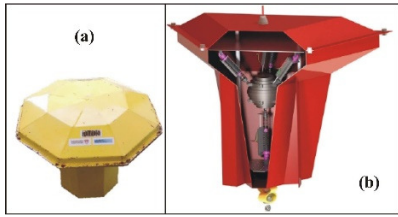

Fig. 1 The TALOS WEC device: (a) TALOS I (Osborne et al., 2015) and (b) TALOS II (Bhatt et al., 2016)

The initial device (TALOS I, Fig. 1a) was developed and tested experimentally by Osborne et al. (2015), while a refined design of the WEC (TALOS II, Fig. 1b), focusing on hull geometry and PTO modifications, was conducted and assessed experimentally by Bhatt et al. (2016). However, further research on the TALOS device is still required including among others, optimization of the hull geometry and of the damper configurations, as well as the design of the mooring system (Aggidis and Taylor, 2017). In order to address all these design challenges, it is necessary to develop integrated time-domain computational tools, that can capture efficiently all the intrinsic dynamic and operational features of the device related to: (a) the coupling effects between the modes of the floater itself as well as between the internal mass and the floater, and (b) the interactions between the various PTO modes of operation.

Motivated by this, the present paper focuses on the preliminary time-domain analysis of the TALOS WEC by deploying two different computational tools. The first one corresponds to an in-house tool developed recently at Lancaster University (Sheng et al., 2022) specifically for the TALOS device, while the second one corresponds to the DNV-SESAM software suite (DNV, 2022). Both tools enable the inclusion in the analysis of the hydrodynamic and the PTO forcing, the hydrostatic-gravitational and mooring system forcing, the DoFs of both the floater and the sphere, as well as all relevant coupling/interaction effects. The equation of motion is formed and solved by deploying the Cummins time-domain formulation (Cummins, 1962), while different approaches between the two tools are applied to calculate the convolution terms. The required for the analysis frequency-depended exciting forces and hydrodynamic coefficients are obtained from the solution of the corresponding diffraction/radiation problem in the frequency domain by utilizing the conventional boundary integral equation method. Initially, a comparative study is conducted to examine the efficiency of the two computational tools and the rationality behind their results. Comparisons are made in terms of the device responses under both regular and irregular waves for a simplified case, where the sphere is assumed to be rigidly attached to the floater (i.e., no operation of the PTO mechanism is considered). Next, by enabling the sphere to oscillate in heave, as well in both heave and surge, and, thus, considering respectively a single- and a two-mode PTO mechanism, the second computational tool is applied to assess the dynamic behavior and power absorption ability of the device under different wave conditions. The present paper contributes to the numerical performance assessment of multi-mode PAs by: (a) highlighting the effect of different numerical schemes related to the convolution terms' calculation, on the solution of the equation of motion and (b) providing an initial figure of the TALOS WEC power absorption level.

NUMERICAL ANALYSIS

Characteristics of the TALOS WEC

TALOS WEC consists of an axisymmetric, octagonal mushroom-shaped floater. The geometry of the floater's wetted surface along with the panel (mesh) discretization used in the hydrodynamic calculations is shown in Fig. 2.
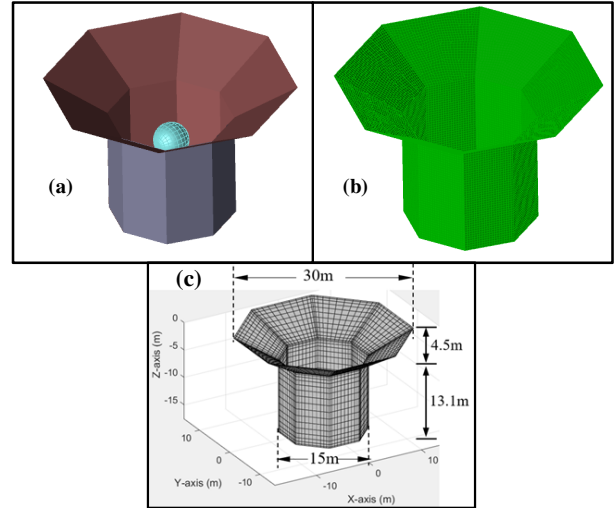

Fig. 2 Geometry of the wetted surface of the TALOS WEC's floater: (a) general view including the sphere, (b) panel discretization, (c) main dimensions

Table 1. Characteristics of the TALOS WEC's floater, internal sphere and mooring system

Floater	
Parameter	**Value**
Draft, h (m)	17.60
Mass, m (kgr)	3,048,620
Displaced volume, V (m³)	3,754.52
Center of mass, CoG (m)	(0,.0, 0.0, -7.9605)
Center of buoyancy, CoB (m)	(0,.0, 0.0, -6.9202)
Moment of inertia, Ixx (kgr m²)	481,500,000.00
Moment of inertia, Iyy (kgr m²)	481,500,000.00
Moment of inertia, Izz (kgr m²)	245,000,000.00
Mooring system equivalent stiffness in surge, K_{11} (N/m)	500,000.00
Mooring system equivalent stiffness in sway, K_{22} (N/m)	500,000.00
Mooring system equivalent stiffness in yaw, K_{66} (N/m)	2,500,000.00
Sphere	
Parameter	**Value**
Mass, m_{sp} (kgr)	800,000
Center of mass, CoG_{sp} (m)	(0.0, 0.0, -5.7)

The floater including the internal sphere has a total draft of 17.6 m. Its diameter remains constant and equal to 15.0 m from the floater's bottom up to 4.5 m below the MWL, and, then, it gradually increases having a value of 30.0 m on the MWL. The sphere (Fig. 2a) is placed inside the floater at 5.7 m below the MWL. More details of the characteristics of the TALOS WEC's floater and internal sphere are cited in Table 1. The draft, mass, displaced volume and center of buoyancy, similar to those of TALOS I, have been defined from hand calculations; however, they were also confirmed with the use of the

DNV-SESAM software suite. The centers of gravity and buoyancy, as well as the moments of inertia are defined with respect to the global $OXYZ$ coordinate system placed on the MWL in the center of the device. It is noted that uniform thickness has been considered for the whole wetted surface of the floater to calculate the floater's characteristics. As for the mooring system, it has been idealized in the present paper to provide linear stiffness in three DoFs, corresponding to surge (motion along OX axis), sway (motion along OY axis) and yaw (rotation around OZ axis). In the rest three DoFs, the restoring forces result from hydrostatic-gravitational contributions.

Description of the Two Computational Tools

In the present paper, the time-domain analysis of the TALOS device is conducted by utilizing two different computational tools: an in-house tool developed recently at Lancaster University specifically for the TALOS device, named herein CT1, and the DNV-SESAM software suite, abbreviated herein as CT2. CT1 is based on the hybrid frequency-time domain approach (Sheng at al., 2022). Specifically, the basic hydrodynamic quantities are obtained in the frequency domain using any relevant solver, and then they are transformed for the time-domain equation. CT2 corresponds to a commercial software suite developed by DNV with extended capabilities for the integrated design and analysis of ships and floating offshore structures (DNV, 2022). This tool has been used to build from scratch a numerical model for the TALOS WEC.

In both tools, the equation of motion is formed based on the Newton's second law by deploying the Cummins time-domain formulation (Cummins, 1962). The latter formulation takes into account the interaction of the wave exciting forces with the radiation forces induced by the motions of the floating structure itself, also known as fluid memory effects. Based on the above and assuming N and M DoFs for the floater and the internal sphere respectively, the equation of motion for the TALOS WEC is defined as follows:

$$\left(\mathbf{M}+\mathbf{A}_\infty\right)\ddot{\mathbf{x}}(t)+\int_{-\infty}^{t}\mathbf{B}(t-\tau)\dot{\mathbf{x}}(\tau)d\tau+\left(\mathbf{C}+\mathbf{K}\right)\mathbf{x}(t)=\mathbf{F}_{\mathbf{exc}}(t)+\mathbf{F}_{\mathbf{PTO}}(t) \quad (1)$$

where $\mathbf{x}$, $\dot{\mathbf{x}}$ and $\ddot{\mathbf{x}}$ are the displacement, velocity and acceleration vectors, $\mathbf{M}$ is the structural mass matrix, $\mathbf{A}_\infty$ is the added mass matrix at infinite frequency, $\mathbf{B}$ is the matrix of impulse response functions, also known as retardation functions, $\mathbf{C}$ is the hydrostatic-gravitational stiffness matrix, $\mathbf{K}$ is the mooring lines stiffness (assuming linear springs), $\mathbf{F}_{\mathbf{exc}}$ is the wave loading vector, $\mathbf{F}_{\mathbf{PTO}}$ is the vector of forces resulting from the PTO mechanism, t is time, while τ is a dummy variable. The maximum dimensions of the above matrices and vectors correspond to $(N+M)$ X $(N+M)$ and $(N+M)$ X 1 respectively.

Cummins' equation is a second order differential equation with a convolution integral in it, which makes the computational solution complicated in time domain (Kashiwagi, 2004). In order to calculate the convolution terms fast and reliably, the impulse response functions in the case of CT1 are approximated using the 16-order Prony function (Sheng et al., 2015). As for CT2, direct solution of the convolution integral was conducted by utilizing the Kramer-Kronig relationship (King, 2009).

The wave exciting forces and hydrodynamic coefficients of the floater for a large set of frequencies, as well as the hydrostatic-gravitational stiffness coefficients are obtained by deploying WAMIT (Lee, 1995) and WADAM module of DNV SESAM (DNV, 2022) in the case of CT1 and CT2 respectively. A panel size sensitivity study has been performed in order all the quantities to be independent from the size of

the panels. Furthermore, the quantities calculated with the two different frequency-domain tools (e.g., WAMIT, WADAM) were compared to ensure the inclusion of the same input in both CT1 and CT2.

RESULTS AND DISCUSSION

Characteristics of Examined Cases

In the present paper, the TALOS WEC is examined for three different operational cases. In the first case (OC1), the analysis is implemented assuming that the PTO mechanism is not operating and that the sphere is rigidly attached to the floater. Accordingly, all DoFs of the sphere are considered ideally restricted, the two bodies (floater and sphere) are moving together without having any relative motions and Eq. 1 is solved by setting M and $\mathbf{F}_{\mathbf{PTO}}$ equal to zero. This simplified operational case is introduced in order to perform a comparative study between the two deployed computation tools with an overall aim to: (a) assess the efficiency of these tools, as well as the rationality behind their outcome and (b) highlight the reasons that can lead to possible differences between their results. In the second operational case (OC2), we account for a single-mode PTO mechanism, by enabling the sphere to oscillate in heave relatively to the floater, while keeping the rest DoFs of the internal mass restrained. Accordingly, Eq. 1 is solved for $M=1$. In OC2, the PTO mechanism of the device is modelled as a linear, 1-DoF, spring-damper system with PTO coefficients included in Table 2. Finally, a two-mode PTO mechanism is considered in the third operational case (OC3), by allowing the sphere to oscillate in surge and heave simultaneously and relatively to the floater and keeping the rest DoFs of the internal mass restrained. Thus, Eq. 1 is solved for $M=2$. The PTO mechanism in OC3 is modelled as a linear, 2-DosF, spring-damper system with coefficients also shown in Table 2.

Table 2. PTO mechanical characteristics of the TALOS WEC for OC2 and OC3

OC	Parameter	Value
OC2 & OC3	Equivalent heave PTO stiffness, $K_{PTO,heave}$ (N/m)	1,250,000
OC2 & OC3	Equivalent heave PTO damping, $B_{PTO,heave}$ (Ns/m)	675,000
OC3	Equivalent surge PTO stiffness, $K_{PTO,surge}$ (N/m)	1,250,000
OC3	Equivalent surge PTO damping, $B_{PTO,surge}$ (Ns/m)	675,000

For all examined cases, the device is placed at 100 m water depth, while the action of head waves is taken into account. Thus, in OC1, OC2 and OC3, Eq. 1 is solved for $N=3$ DoFs corresponding to the floater's surge, heave and pitch motions along OX, OZ and around OY axis respectively.

Comparative Study between the Two Computational Tools for OC1

The comparative study for OC1 is implemented under the action of both regular and irregular waves, with characteristics included in Table 3. For the regular wave conditions (EC1-EC3 in Table 3), the wave height, H, is taken equal to 2.0 m, while the period, T, is set equal to 10.0 s, 8.5 s and 7.0 s. For the irregular wave condition (EC4 in Table 4), the Jonswap spectrum with peakedness factor of 1.0 (i.e., Bretschenider spectrum) has been used with significant wave height, H_s, and peak period, T_p, equal to 2.0 m and 10.0 s respectively. The total simulation time is 400 s for the regular wave conditions and 3,600 s for the irregular wave condition.

Table 3. Environmental conditions for the comparative study

Environmental Conditions	Wave height (m)	Period (s)	Type of wave
EC1	2.0	10.0	Regular
EC2	2.0	8.5	Regular
EC3	2.0	7.0	Regular
EC4	2.0	10.0	Irregular

As mentioned in the previous section, first-order exciting forces, added mass and radiation damping coefficients required for the time-domain analysis have been obtained using WAMIT and WADAM for CT1 and CT2 respectively. The inclusion of the same input in both computational tools was ensured, since the comparison of the exciting forces (amplitude and phase in all DoFs), as well as of the added mass and the radiation damping coefficients (for all DoFs and for coupling terms), showed minor differences (smaller than 1%) between the two frequency-domain tools. Fig. 3 shows indicatively the variation of the surge (F_1), heave (F_3) and pitch (F_5) exciting forces as a function of the frequency ω, as well as the corresponding variation of the surge and heave added mass (A_{11}, A_{33}) and radiation damping (B_{11}, B_{33}) coefficients of the TALOS WEC, as obtained from WADAM.
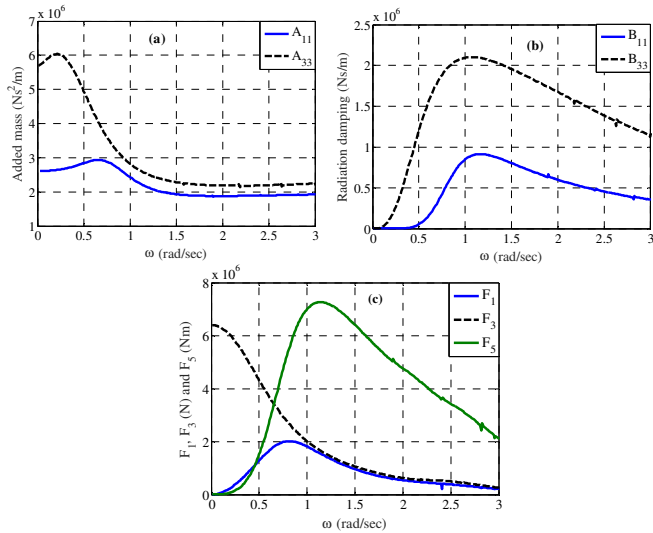

Fig. 3 Frequency-depended quantities of TALOS WEC: (a) surge and heave added mass coefficients, (b) surge and heave radiation damping coefficients and (c) exciting forces

For including memory effects, impulse response functions have been estimated by deploying different numerical schemes in the two computational tools (sum of complex exponentials using Prony's method in CT1 and direct solution of the convolution integral in CT2). Fig. 4 shows a comparison of the surge, heave, pitch and surge-pitch impulse response functions as calculated in the two time-domain tools. It can be seen that the application of different numerical schemes for the impulse response functions' estimation introduces differences for all the DoFs, but also for the coupled term.

With regard to the responses of the TALOS WEC, Fig. 5 shows the comparison of the surge (Fig. 5b), heave (Fig. 5c) and pitch (Fig. 5d) motions as obtained from CT1 and CT2 for EC1. A comparison of the wave elevation is also included in this figure (Fig. 5a). The latter quantity is the same between the two computational tools resulting to the same wave exciting forces for both CT1 and CT2. In the case of the

uncoupled heave motion (Fig. 5c), an excellent agreement between the two computational tools is obtained, taking also into account that the heave impulse response functions among CT1 and CT2 show small differences (Fig. 4b). With regards to the rest two motions (surge and pitch) that are coupled, larger differences compared to the heave motion are observed. Pitch motion (Fig. 5d) obtains similar values between the two different tools, with small differences, occurring mainly close to the curves' peaks, due to the existence of differences in the pitch impulse response function (Fig. 4c). However, for the surge motion (Fig. 5b) the differences become larger. This fact is attributed to the differences observed not only for the surge impulse response functions (Fig. 4a), but also for the coupled surge-pitch impulse response functions (Fig. 4d), which have values around ten times larger than the surge ones. It is noted that the time variation of the surge response is affected by both the incident wave period (i.e., $T=10.0$ s) as well as by the surge natural period of the device, which has been calculated equal to 21.26 s for the characteristics of the mooring system included in Table 1.
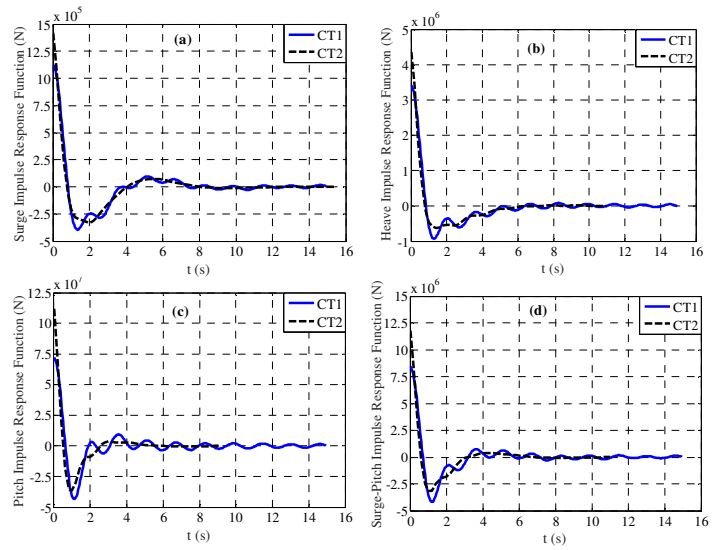

Fig. 4 Comparison of impulse response functions of: (a) surge, (b) heave, (c) pitch and (d) surge-pitch
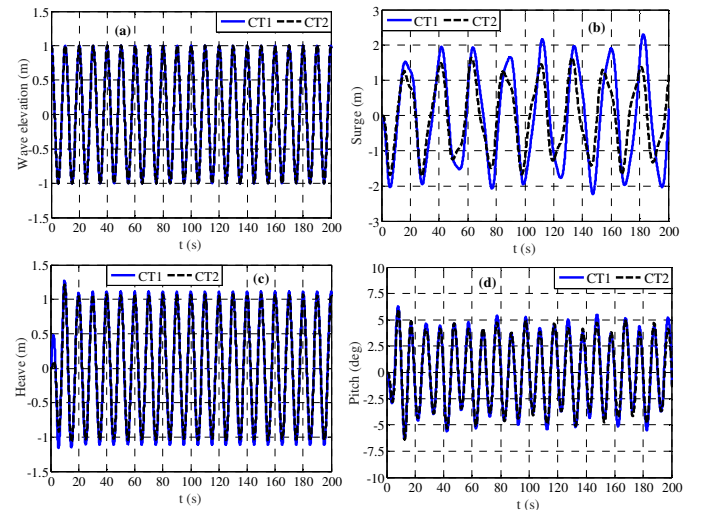

Fig. 5 Comparisons between CT1 and CT2 for EC1: (a) wave elevation, (b) surge, (c) heave and (d) pitch

For the rest two regular wave conditions (EC2 and EC3), analogous conclusions can be derived regarding the comparison of the device's motions. This is illustrated in Fig. 6, which shows the comparison between CT1 and CT2 for EC2 indicatively for surge and pitch (Figs. 6a, 6b) and for EC3 in terms of heave and pitch (Figs. 6c, 6d). It can be seen that the heave and pitch motions between the two computational tools are similar, while larger differences are still observed in the case of surge due to the differences introduced in the coupled surge-pitch impulse response functions (Fig. 4d).
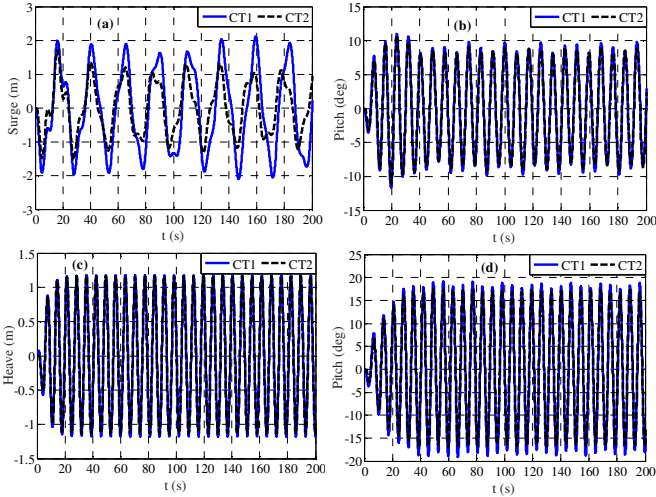
Fig. 6 Comparisons between CT1 and CT2 for EC2 and EC3: (a) surge (EC2), (b) pitch (EC2), (c) heave (EC3) and (d) pitch (EC3)

Finally, with regard to the irregular wave condition examined (EC4), in Fig. 7 the comparison of the wave elevation (Fig. 7a), the surge (Fig. 7b), the heave (Fig. 7c) and the pitch (Fig. 7d) motions between CT1 and CT2 is shown for part of the whole simulation time. It is apparent that similar values are obtained for both CT1 and CT2 in the case of heave and pitch, while for surge differences are observed for the reasons previously explained.
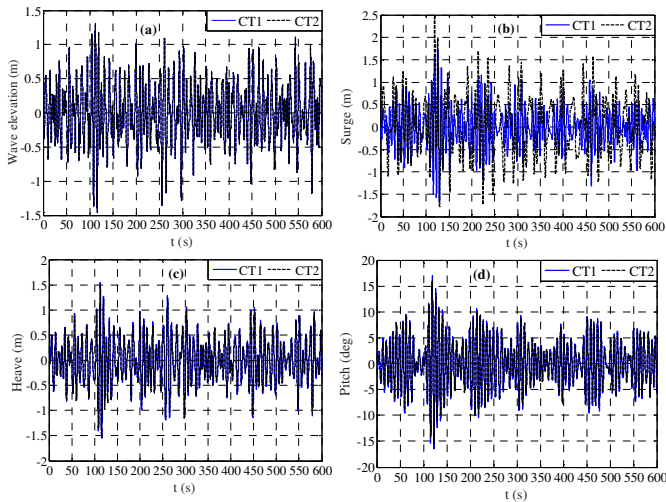

Fig. 7. Comparisons between CT1 and CT2 for EC4: (a) wave elevation, (b) surge, (c) heave and (d) pitch

TALOS WEC Responses for OC2 and OC3

The time-domain analysis for OC2 (single-mode PTO mechanism) and OC3 (two-mode PTO mechanism) has been conducted for the environmental conditions of Table 3 by deploying only the second computational tool (CT2).

Staring with OC2, Fig. 8 shows the floater's surge and pitch motions (Fig. 8a), as well as the heave motion of both the floater and the sphere (Fig. 8b) indicatively for EC1. From the latter figure, it is apparent that the heave motion of the sphere has the same time-variation pattern and it is in phase with the floater's heave motion; however, differences in the values of the heave responses between the two bodies are observed. Analogous conclusions can be drawn for EC2 and EC3 (results are not included here due to space constraints). Accordingly, relative heave motion between the floater and the sphere for all regular wave conditions examined do exist (Fig. 9), with values depending upon: (i) the structural features of the internal mass (Table 1), (ii) the single-mode PTO stiffness and damping coefficients (Table 2) and (iii) the incident wave characteristics. Regarding the latter parameter, the results of Fig. 9 demonstrate that the decrease of T in EC2 leads to larger relative heave motions between the two bodies compared to EC1. This trend is more pronounced in the case of EC3, where the smallest wave period equal to 7 s has been taken into account.
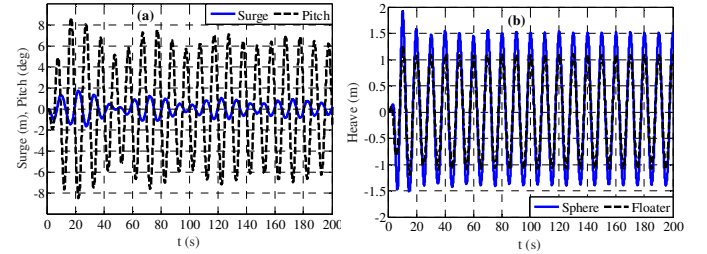

Fig. 8 Motion responses for OC2 and EC1: (a) floater's surge and pitch and (b) floater's and sphere's heave
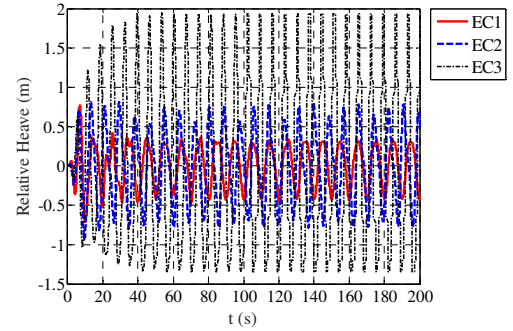

Fig. 9 Relative heave motion between the floater and the sphere for OC2 and EC1, EC2 and EC3

With regards to the irregular wave condition (EC4), Fig. 10 includes parts of the time series of the floater's and sphere's responses, while the corresponding response spectra are shown in Fig. 11. The existence of relative heave motion between the floater and the sphere is again observed (Fig. 10c) with maximum, minimum and standard deviation values equal to 1.4 m, -1.863 m and 0.394 m, respectively. As for the response spectra (Fig. 11), it can be seen that the spectra of all the floater's motions have high energy content at the resonance frequency regions (between 0.05 Hz and 0.15 Hz) and close to the peak frequency (0.1 Hz) of the incident wave spectrum (Fig. 11a). The heave response

spectrum of the sphere is similar with that of the floater's heave response (Fig. 11c); however, it shows a larger energy content when compared to the heave spectrum of the floater.
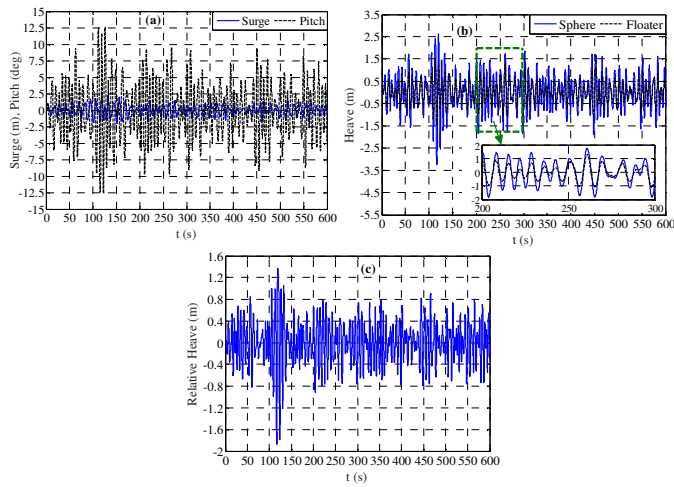

Fig. 10 Motion responses for OC2 and EC4: (a) floater's surge and pitch, (b) floater's and sphere's heave and (c) relative heave motion between the two bodies
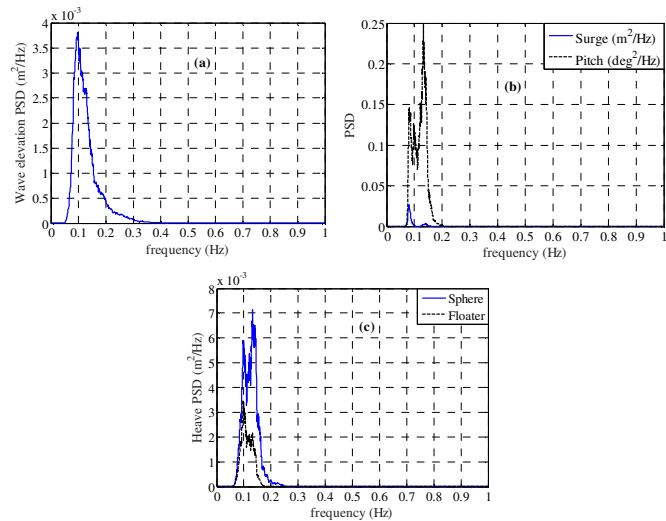

Fig. 11 OC2 and EC4: (a) incident wave spectrum, (b) floater's surge and pitch spectra, (b) floater's and sphere's heave spectra (PSD: Power Spectral Density)

Continuing with OC3, the floater's and the sphere's responses are presented in Fig. 12 indicatively for EC1. The variation pattern of the floater's surge, heave and pitch motions are similar with those obtained in OC2, while, furthermore, the sphere's both surge and heave motions are in phase with the corresponding ones of the floater. Similar conclusions can be derived for EC2 and EC3 (results are not included here due to space constraints). Based on Figs. 12a and 12b, it can be concluded that for the specific environmental condition the relative motion between the two bodies is more pronounced in the heave DoF compared to the surge one. This is also illustrated in Figs. 13-14, where the relative surge (Fig. 13) and heave (Fig. 14) motions between the floater and the sphere for all examined regular wave conditions are shown.
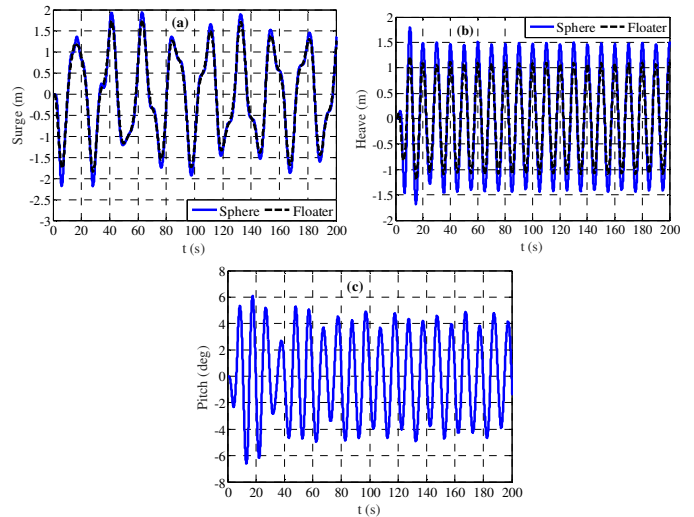

Fig. 12 Motion responses for OC3 and EC1: (a) floater's and sphere's surge, (b) floater's and sphere's heave and (c) floater's pitch

Taking into account the results of Figs. 13-14, it is apparent that the incident wave period, which varies among EC1, EC2 and EC3, has a direct effect on the relative motions between the two bodies. Specifically, in the case of the heave relative motion (Fig. 14), the decrease of T in the case of EC2 leads to larger values compared to EC1. The same holds true for EC3, where the relative heave response show insignificant differences compared to that of EC2. As for the relative surge motion (Fig. 13), a small increase of this quantity is observed in the case of EC2 compared to EC1. This increase, however, becomes quite significant for EC3, due to the resonance of the floater's pitch motion and the coupling of this DoF with the surge one.
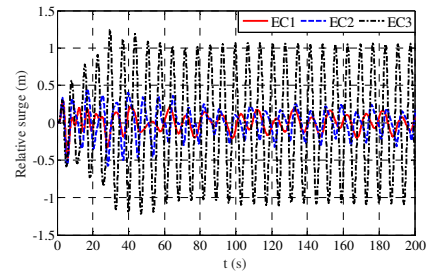

Fig. 13 Relative surge motion between the floater and the sphere for OC3 and EC1, EC2 and EC3
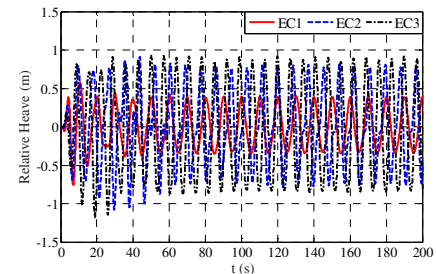

Fig. 14 Relative heave motion between the floater and the sphere for OC3 and EC1, EC2 and EC3

Finally, the results for OC3 under the action of irregular waves (EC4) are presented in Fig. 15. As in the case of regular waves, the relative

heave motion between the two bodies obtains larger values compared to the relative surge motion.
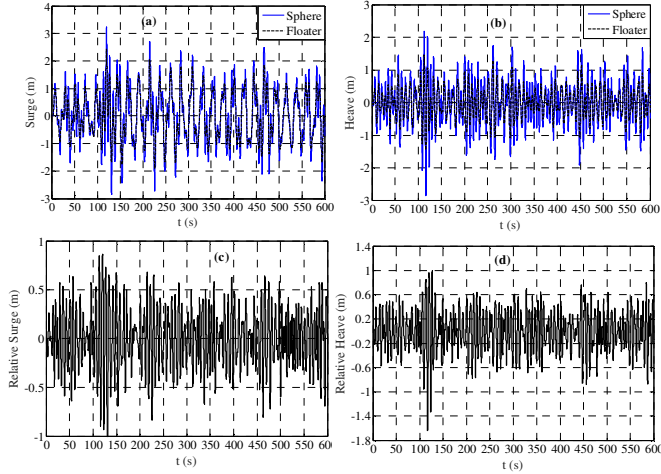

Fig. 15 Motion responses for OC3 and EC4: (a) floater's and sphere's surge, (b) floater's and sphere's heave, (c) relative surge motion between the two bodies and (d) relative heave motion between the two bodies

TALOS WEC Absorbed Power for OC2 and OC3

In this section, the power absorbed by the TALOS WEC for both OC2 and OC3 under the action of irregular waves (EC4) is assessed. Assuming a linear, 1-DoF (OC2) and 2-DoFs (OC3) PTO system, the power absorbed by the device, *Power*, is calculated using Eqs. 2 and 3 for OC2 and OC3 respectively:

$$Power(t) = B_{PTO,heave}\left(\dot{x}_{hf}(t) - \dot{x}_{hs}(t)\right)^2 \qquad (2)$$

$$Power(t) = B_{PTO,surge}\left(\dot{x}_{sf}(t) - \dot{x}_{ss}(t)\right)^2 + B_{PTO,heave}\left(\dot{x}_{hf}(t) - \dot{x}_{hs}(t)\right)^2 \quad (3)$$

In the above equations, $\dot{x}_{sf}$, $\dot{x}_{hf}$ are the velocities of the floater in surge and heave respectively, while $\dot{x}_{ss}$ and $\dot{x}_{hs}$ are the corresponding quantities for the sphere. Those velocities are obtained from the solution of Eq. 1 (for example, $\dot{x}_{sf}$ and $\dot{x}_{hf}$ correspond to $\dot{x}_1$ and $\dot{x}_2$ in Eq. 1).

Fig. 16 shows the time variation of the power absorbed by the TALOS device for OC2 (Fig. 16a) and for OC3 (Figs. 16b-16d). In the latter case, additional to the total power (Fig. 16b), the power absorbed separately in each DoF of the PTO is also presented (Figs. 16c-16d). In the case of OC2 (Fig. 16a), the consideration of the one-mode PTO mechanism operating only in heave, leads to mean absorbed power equal to 102.0 kW. As far as OC3, the aforementioned quantity resulting from the surge DoF (Fig. 16c) and the heave DoF (Fig. 16d) of the PTO is equal to 66.8 kW and 81.43 kW respectively; this, in turn, demonstrates that for the wave conditions, the PTO and the sphere characteristics considered in the present paper, the absorbed power in heave is a bit larger compared to the power absorbed in the second (surge) operational mode. As for the total power absorbed by the device (Fig. 16b), its mean value for OC3 is equal to 148.2 kW, corresponding approximately to a 45% relative increase compared to OC2. Accordingly, it can be concluded that the deployment of the two-mode PTO mechanism increases the power absorption ability of the device.
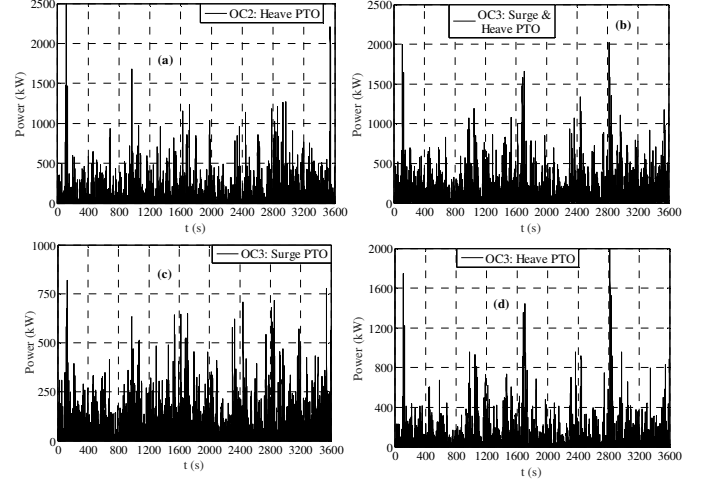

Fig. 16 Absorbed power for EC4: (a) OC2 (total), (b) OC3 (total), (c) OC3 (only from the surge PTO DoF) and (d) OC3 (only from the heave PTO DoF).

CONCLUSIONS

In this paper, a preliminary time-domain analysis of the TALOS multi-mode WEC by deploying two different computational tools has been performed and presented. The analysis was conducted for three different, with increasing complexity, operational conditions of the device's PTO mechanism under the action of both regular and irregular waves. A comparative study between the two tools was realized assuming rigid connection of the sphere with the floater. Next, by enabling the sphere to oscillate in heave, as well as in both heave and surge, the performance of the device was assessed for one and two operational modes of the PTO under various wave conditions.

The results of the comparative study demonstrated that both computational tools are capable to generate rational results and can be considered efficient for the analysis of the TALOS WEC in time-domain. The observed between the two computational tools differences in the response of the device were attributed to the deployment of different numerical schemes to quantify the impulse response functions. For the characteristics of the problem examined in the present paper, those differences were pronounced in the case of the floater's surge motion, mainly due to the dissimilarities of the coupled surge-pitch impulse response functions among the two tools.

Regarding the performance of the device for the one- and the two-mode PTO mechanism, the results for the regular wave conditions illustrated that the incident wave period has a direct effect on the relative motions between the floater and the sphere. On the other hand, under irregular waves, the operation of the TALOS WEC in a multi-mode way results to a significant increase of the absorbed power, without affecting the rest responses.

The computational tools of the present paper could be further developed in order to account for an appropriate mooring system and/or a PTO mechanism with more than two DoFs. Accordingly, the effect of various design parameters of the TALOS device on its performance can be investigated, as well as a mooring system can be designed in an efficient way. The comparison of numerical results with experimental ones in terms of validating and enhancing the two computational tools of this paper presents also an item for future research.

REFERENCES

Aggidis, GA, and Taylor, CJ (2017). "Overview of Wave Energy Converter Devices and the Development of a New Multi-axis Laboratory Prototype," *IFAC-PapersOnLine*, 50(1), 15651–15656.

Bhatt, J, Carthy, J, Clark, T, Galea, S, Sutch, A, Tutt, A, and Walker, J (2016). *Optimisation and Development of A Multi-Axis Wave Energy Converter Device*, Master of Engineering Project Report, Engineering Department, Lancaster University, 289.

Collombet, R, and Cagney, D (2022). *Last Stop to 2025: A 2022 Action Plan to Deliver on the Offshore Strategy's Ocean Energy Target*, Ocean Energy Europe, 24.

Cummins, WE (1962). *The Impulse Response Function and Ship Motions*, Report 1661, Department of the Navy David Taylor Model Basin, 12.

Det Norske Veritas (DNV) (2022). *Sesam Software Suite for Hydrodynamic and Structural Analysis of Renewable, Offshore and Maritime Structures*, Digital Solutions at DNV, 253.

European Commission (2020). *Communication from the Commission to the European Parliament, the Council, the European Economic and Social Committee and the Committee of the Regions: an EU Strategy to Harness the Potential of Offshore Renewable Energy for a Climate Neutral Future*, European Commission, 27.

Guo, B, and Ringwood, JV (2021). "A Review of Wave Energy Technology from a Research and Commercial Perspective," *IET Renew Power Gener*, 15, 3065–3090.

Guo, B, Wang, T, Jin, S, Duan, S, Yang, K, and Zhao, Y (2022). "A Review of Point Absorber Wave Energy Converters," *J Mar Sci Eng*, 10, paper No. 1534.

Huang, S-T, Shi, H-D, and Dong, X-C (2019). "Capture Performance of a Multi-Freedom Wave Energy Converter with Different Power Take-off Systems," *China Ocean Eng*, 33(3), 288–297.

Kashiwagi, M (2004). "Transient Responses of a VLFS during Landing and Take-off of an Airplane," *J Mar Sci Tech*, 9(1), 14–23.

King, F (2009). *Hilbert Transforms*. Cambridge: Cambridge University Press.

Lee, CH (1995). *WAMIT Theory Manual*, MIT Report 95-2, Department of Ocean Engineering, MIT, 66.

Osborne, J, Rawcliffe, P, Tarrant, H, Wheatland, W, Lovett, M, Tailyour, J, Veryard, P, Woodall, A, and Jesson, P (2015). *Multi-axis Wave Energy Converter*, Master of Engineering Project Report, Engineering Department, Lancaster University, 515.

Rusu, E, and Onea, F (2018). "A Review of the Technologies for Wave Energy Extraction," *Clean Energy*, 2(1), 10–19.

Sheng, W, Alcorn, R, and Lewis A (2015). "A New Method for Radiation Forces for Floating Platforms in Waves," *Ocean Eng*, 105, 43–53.

Sheng, W, Tapoglou, E, Ma, X, Taylor, CJ, Dorrell, R, Parsons, DR, and Aggidis, G (2022). "Time-Domain Implementation and Analyses of Multi-Motion Modes of Floating Structures," *J Mar Sci Eng*, 10(5), paper No. 662.

Tan, M, Cen, Y, Yang, Y, Liu, X, Si, Y, Qian, P, and Zhang D (2021). "Power Absorption Modelling and Analysis of a Multi-axis Wave Energy Converter," *IET Renew Power Gener*, 15, 3368–3384.

Ye, Y, and Chen, W (2017). "Frequency- and Time-domain Analysis of a Multi-Degree-of-Freedom Point Absorber Wave Energy Converter," *Adv Mech Eng*, 9(12), 1–10.

Zhang, D, Aggidis, G, Wang, Y, Gu, X, Li, W, and Chen, Y (2015). "Wave Tank Experiments on the Power Capture of a Multi-axis Wave Energy Converter," *J Mar Sci Technol*, 20, 520–529.

Zhang, D, Aggidis, G, Wang, Y, Mccabe, A, and Li, W (2013). "Experimental Results from Wave Tank Trials of a Multi-axis Wave Energy Converter," *Appl Phys Lett*, 103(10), paper No. 103901.